JOURNAL OF GEOPHYSICAL RESEARCH, VOL. 112, C04S12, doi:10.1029/2006JC003735, 2007

On the boundary conditions applied to the sea-ice coupled model

Rui Xin Huang[1] and Xiangze Jin[1]

Received 30 May 2006; revised 7 December 2006; accepted 19 January 2007; published 6 April 2007.

[1] The formulation of suitable boundary conditions at the water-ice interface during ice formation (melting) is an important aspect of the sea-ice coupled model. The transfer of water and salt through the water-ice can be posed as different boundary conditions. Behavior of the model under these boundary conditions is illustrated through simple analytical models and a numerical model based on pressure-η coordinate. It is emphasized that the correct handling of the boundary conditions associated with sea ice formation requires an accurate treatment of the equivalent pressure on the top of water column and the total volume (mass) of the water column in the ice formation regime. Improper treatment of these boundary conditions may lead to an artificial loop current near the edge of ice in numerical simulations of oceanic circulation in the Arctic Ocean or near the Antarctica.

Citation: Huang, R. X., and X.-Z. Jin (2007), On the boundary conditions applied to the sea-ice coupled model, *J. Geophys. Res.*, *112*, C04S12, doi:10.1029/2006JC003735.

1. Introduction

[2] Boundary conditions suitable for simulating freshwater flux through the air-sea interface have been discussed in many publications. (In this study, the word "interface" means the vertical interface between either the air and sea or the ice and water below.) Three types of boundary conditions have been used in oceanic general circulation models, including the traditional relaxation condition, the virtual salt flux condition, and the natural boundary condition. The advantage and limitations of these boundary conditions have been discussed in previous publications [e.g., *Huang*, 1993; *Roullet and Madec*, 2000].

[3] Ice formation (melting) is a critically important aspect of oceanic circulation in high latitude oceans, including both the Arctic and the Southern Ocean. During ice formation (melting) there are freshwater and salt exchanges across the water-ice interface, and the corresponding boundary conditions at the water-ice interface were discussed in previous literatures [i.e., *Tartinville et al.*, 2001; *Zhang and Zhang*, 2001; *Prange and Gerdes*, 2006].

[4] In this study, we will examine the physical processes associated with ice formation and salt rejection. Since ice formation is intimately related to water-ice interfacial mass exchange, including both water and salt, a careful handling of changes in volume or mass of the ocean model and changes in pressure is critically important for the accurate simulation of oceanic environments associated with ice formation (melting).

[5] We begin with the study of these physical processes in a simple slab model. In order to find analytical solutions, this problem is explored in light of the geostrophic adjustment in section 2. The accurate simulation of ice formation (melting) requires running oceanic general circulation models (OGCM); thus, suitable boundary conditions for OGCM, including the virtual salt flux condition and the natural boundary conditions for the water-ice interface are discussed in section 3. These boundary conditions are tested in numerical experiments with simple geometry for several cases in section 4. The final conclusions are drawn in section 5.

2. Ice Formation and the Associated Boundary Conditions

[6] Ice formation can induce horizontal imbalance of pressure in the water column below ice due to salt rejection. The ocean is thus driven by the initial pressure gradient force toward a new equilibrium state. Geostrophic adjustment of a slab/layer model in the ocean has been discussed in many papers. Our notation here is parallel to that of *Mihaljan* [1963] and *Huang and Jin* [2002]. For simplicity, we will assume that a slab of sea ice is instantaneously formed. In addition, sea ice formation is idealized into two types: the sea ice formation with or without salt rejection. Salt rejection induces a baroclinic circulation which is relatively weak. However, two major problems related to ice formation exist. First one is how to treat the exchange of freshwater and salt fluxes across the water-ice interface? Second one is how to deal with change in pressure on the upper surface of the water column?

[7] A commonly used approach is to treat the ice formation in terms of an equivalent salt flux due to salt rejection and ignore pressure change on the upper surface of the water column. The limitations of the virtual salt flux condition used to simulate evaporation and precipitation was discussed by *Huang* [1993]. One of the major problems associated with the virtual salt flux condition for evaporation and precipitation is due to the fact that the global mean

[1]Department of Physical Oceanography, Woods Hole Oceanographic Institution, Woods Hole, Massachusetts, USA.

0148-0227/07/2006JC003735$09.00

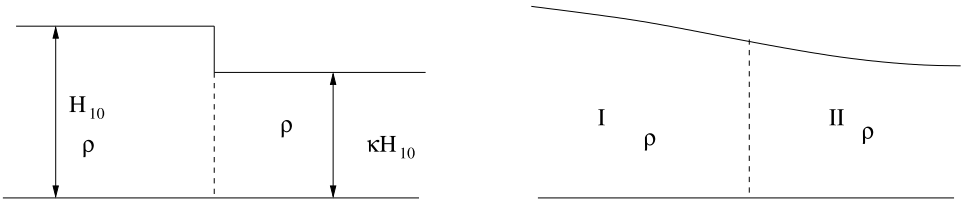

a) An initial step in sea surface level.

b) The sea surface level after adjustment.

Figure 1. Sketch of the layer thickness distribution (a) before and (b) after adjustment, where H_{10} is the unperturbed layer thickness, and $\kappa H_{10} = (1 - h_w / H_{10})H_{10}$ is the layer thickness after remove of water due to ice formation, without salt rejection. y axis is pointed northward.

salinity has to be used in parameterizing the virtual salt flux. As a result, such a boundary condition exaggerates the dynamic impact of surface freshwater flux. Since surface salinity in an ice-covered ocean tends to be much lower than the global-mean salinity, using the virtual salt flux condition can substantially exaggerate the dynamic impact of ice formation/melting. Therefore, virtual salt flux used for the water-ice interfacial exchange shares pitfalls similar to the virtual salt flux used for evaporation and precipitation.

[8] The second approach is to treat the freshwater/salt fluxes through the water-ice interface in terms of the so-called natural boundary conditions. For a model with a rigid-lid, the natural boundary condition used for evaporation and precipitation was discussed by *Huang* [1993]. This boundary condition can be readily generalized to the model with a free surface and it is now widely used in oceanic general circulation models. However, the corresponding natural boundary condition for ice formation (melting) is slightly more complicated as discussed below.

[9] The ice formation is similar to evaporation because certain amount of freshwater is removed from the water column, which may be parameterized as an equivalent vertical velocity on the top of water column. There is, however, a major difference between ice formation and evaporation. Freshwater associated with evaporation is diffused into the atmosphere where horizontal motions continuously redistribute air mass and thus render the local atmospheric pressure over the seawater nearly unchanged. The remove of freshwater from the upper surface induces current in the ocean which fills up the space left behind by evaporation. The steady barotropic component of the evaporation/precipitation induced motions is the so-called Goldsbrough-Stommel circulation [*Goldsbrough*, 1933; *Stommel*, 1994; *Huang and Schmitt*, 1993].

[10] On the other hand, freshwater across the water-ice interface during ice formation does not entirely disappear from the mass and pressure balance of the local water column. In fact, if we neglect the horizontal movement of sea ice and treat the ice formation as a one-dimensional problem, the same amount of mass and thus the same pressure force remain in effect for the local water column. Therefore, although ice formation can be parameterized in terms of an equivalent evaporation and a remove of freshwater from the water component of the model ocean, the equivalent pressure on the top of water must be increased accordingly. This increase of equivalent pressure on the top of water prevents the lateral movement of water to fill up the space originally occupied by water which is now turning into ice. In fact, if an ocean is initially at rest, ice formation without salt rejection should induce no motion in the ocean at all. Because of the Archimedean principle, there is no horizontal pressure gradient at the base of sea ice, so there is no motion. In conception, if one treats the ice formation in terms of removing of freshwater from the upper surface, but without increasing the pressure on the top of water column, there would be horizontal movement of water to fill up the space left behind during the ice formation. The potential problem connected with such a mishandling of the water-ice interface boundary condition can be readily seen through analyzing a simple slab model, without or with salt rejection during sea ice formation.

2.1. Slab Models

[11] Ice formation can be simulated in terms of simple slab models, and the corresponding solutions can be found analytically. Four simple models are formulated as follows. The analytical details of these models are discussed in Appendix A.

[12] First, assume that a layer of seawater, h_w, is suddenly transformed to sea ice, a step-like feature is thus created at the initial time, Figure 1a. The space left behind will be filled with seawater flowing horizontally, Figure 1b. In this model, density of seawater is assumed constant because no salt rejection is considered, and this model is called SL0. A complete list of slab models discussed in this study is in Table 1.

[13] Second, salt rejection associated with ice formation is considered. As a result, after ice formation water below

Table 1. List of Slab Models Used in This Study

Names	Definition
SL0	Seawater removed, without salt rejection; ignoring increase of pressure on the top of seawater due to ice formation
SL1	Seawater removed, with salt rejection, ignoring increase of pressure on the top of seawater due to ice formation
SL2	Ice formation treated in terms of a virtual salt flux into the water below, but ignoring water flux
SL3	Accurate boundary conditions for freshwater/salt flux and pressure at the ice-water interface

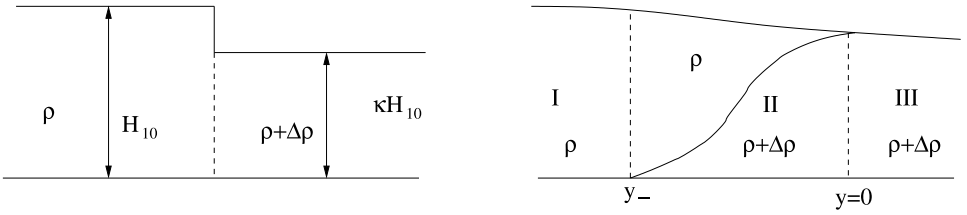

a) An initial step in sea surface level, including salt ejection.

b) The sea surface level after adjustment.

Figure 2. Sketch of the layer thickness distribution (a) before and (b) after adjustment, where H_{10} is the unperturbed layer thickness, $\kappa H_{10} = [1 - (h_w + \delta h)/H_{10}]H_{10}$ and $\rho + \rho\Delta$ are the layer thickness and density after ice formation and salt rejection. y axis is pointed northward.

sea ice is slightly heavier. After the removing of water due to ice formation, the model ocean adjusts accordingly, as shown in Figure 2. This model is called SL1.

[14] Third, a small modification of the SL1 can be used for the case when the ice formation is simulated in terms of the so-called virtual salt flux. Such a model will be referred as the SL2.

[15] Fourth, we set the pressure on the water column below sea ice to the hydrostatic pressure due to the weight of sea ice on top. This case will be referred as model SL3. The adjustment of the model ocean is sketched in Figure 3.

2.2. Comparison of Solutions Under Different Assumptions

[16] Geostrophic adjustment induced by sea ice formation appears in quite different forms under different assumptions, as discussed in Appendix A. In order to demonstrate the difference between these cases, we calculated solutions of these models for two sets of parameters. Case A is a shallow sea with depth of 100 m and 1 m of ice formation, so that the structure of the frontal zone can be viewed clearly, Figures 4 and 5 and Table 2. Case B is for an ocean 1000 m deep with 1 m of ice formation, and this is a more realistic parameter set for the ocean, Table 3.

[17] For SL1 water is pushed towards the ice zone because the initial drop in water level due to ice formation. Thus, in the ice-free region sea level is lower than the initial value, but in the ice-covered region it is higher than the initial value, Figure 4a. The southward movement of water turns to the right (in the Northern Hemisphere) due to the Coriolis force. As a result, geostrophic velocity in the ice-free and the ice-covered regions are all positive. However there is a frontal region associated with the ice edge, where two layers are in baroclinic motions, and there is a tiny zone where the lower layer velocity is negative, Figure 5a.

[18] In contrast, sea level anomaly after adjustment in SL2 and SL3 is opposite to that in SL1. In fact, sea level increases slightly in the ice-free region and declines slightly in the ice-covered regime, Figures 4b and 4c. Changes in sea level are due to the fact that salt rejection creates slightly dense water below the ice, and this density difference pushes the slightly saltier water below ice to the ice-free zone. As a result, there is a weak westward velocity in the far field, Tables 2 and 3.

[19] Regardless of the difference in the far field velocity structure, there are frontal zones in all these models, Figure 5. For both SL3 and SL2 the total volume transport associated with ice formation is small, equal to -0.66 Sv and -0.79 Sv respectively. As discussed in Appendix B, the salinity difference is set to $S - S_1 = 30 - 5 = 25$ for SL3, but is $\bar{S} - S_1 = 30 - 5 = 25$ for SL2. Thus, the ratio of the volume transports is equal to the ratio of salinity difference used in calculating the density difference due to salt rejection.

[20] On the other hand, for model SL1 ice formation can induce a strong barotropic flow. For an ocean 1000 m deep, one meter ice formation may induce a current system with a volume flux of 65 Sv. If the ocean is even deep, this

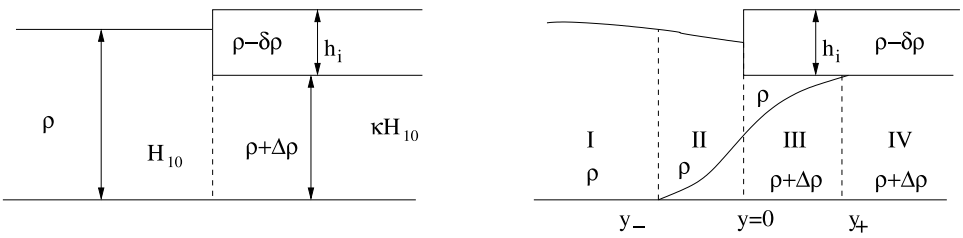

a) An initial step in sea level, including salt ejection after ice formation.

b) The sea surface level after adjustment.

Figure 3. Sketch of the layer thickness distribution (a) before and (b) after adjustment, with a block of sea ice on the top of seawater, where H_{10} is the unperturbed layer thickness, $\kappa H_{10} = [1 - (h_w + \delta h)/H_{10}]H_{10}$ and $\rho + \rho\Delta$ are the layer thickness and density after ice formation and salt rejection. y axis is pointed northward.

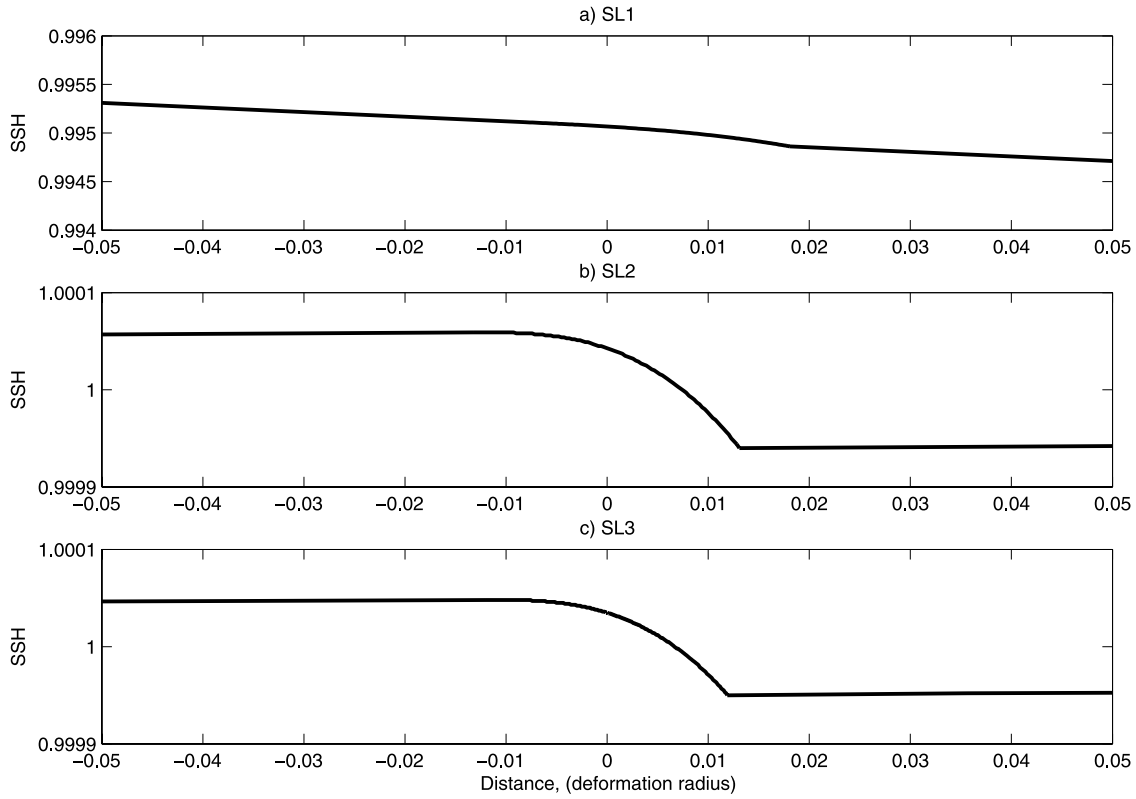

Figure 4. SSH (sea surface height, nondimensional) for water originated from the ice-free zone (to the left) and water originated from the ice-covered zone (to the right) after adjustment for models (a) SL1, (b) SL2, and (c) SL3 in Case A. SSH was set to 1 in the initial state before ice formation. The origin of the ordinate is the edge of ice. Note that for both SL2 and SL3, the free surface elevation in the ice-free zone is slightly pushed upward during the adjustment.

artificial current should be stronger. The dynamic impact of such an artificial current is clearly not negligible.

3. Numerical Model Formulation

3.1. Upper Boundary Conditions for Freshwater Flux

[21] In our previous study [*Huang et al.*, 2001] a pressure-σ coordinate system that conserves mass exactly is adopted. The model was used for a study of idealized cases with a flat bottom. When realistic topography was used, however, errors associated with the horizontal pressure gradients became noticeably larger. Thus, in order to overcome the pressure gradient error typically for low-resolution simulations based on σ-coordinate models, we reformulated our model in pressure-η coordinates [*Huang and Jin*, 2007], which will be called PCOM (Pressure Coordinate Ocean Model) in this study. The PCOM has an option that may be switched to a Boussinesq η-coordinate Ocean Model (BCOM [*Huang et al.*, 2001]), which was also used in this study. The basic concept of η-coordinates and its application to atmospheric/oceanic circulation modeling can be found in *Mesinger and Janjic* [1985] and *Zhang et al.* [2003]. The vertical coordinate pressure-η is defined as

$$\eta = (p - p_t)/r_p, r_p = p_{bt}/p_B,\ p_{bt} = p_b - p_t \tag{1}$$

where $p_b = p_b(x, y, t)$ is the bottom pressure, $p_t = p_t(x, y, t)$ is the hydrostatic pressure at the upper surface of the water column, and $p_B = p_B(x, y)$ is the time-invariant reference bottom pressure, which is calculated from the basin-averaged stratification prescribed in the initial state.

[22] In an ocean-sea ice coupled model, the equivalent pressure on the upper surface of seawater in the ice-covered regime is

$$p_t = p_a + p_i, p_i = \rho_i g h_i \tag{2}$$

where p_a is the sea level atmospheric pressure (assuming constant in this study), p_i is the pressure of the sea ice (g is the gravity, ρ_i and h_i are the density and thickness of the sea ice). Here we assume that ice covers the whole surface of a grid box with an average thickness h_i. This formulation can be used to handle a situation with thick sea ice. For example, huge ice burgs are separated from the Antarctica (or Greenland) with thickness of a few hundred meters, which can be easily simulated in the pressure-η coordinate model or the z-σ coordinate model, but it would be rather difficult to deal with in the traditional z-coordinate models.

[23] In the pressure-η coordinate the continuity equation is

$$\frac{\partial r_p}{\partial t} + \frac{1}{a\cos\theta}\left(\frac{\partial r_p u}{\partial \lambda} + \frac{\partial r_p v \cos\theta}{\partial \theta}\right) + \frac{\partial r_p \dot{\eta}}{\partial \eta} = 0 \tag{3}$$

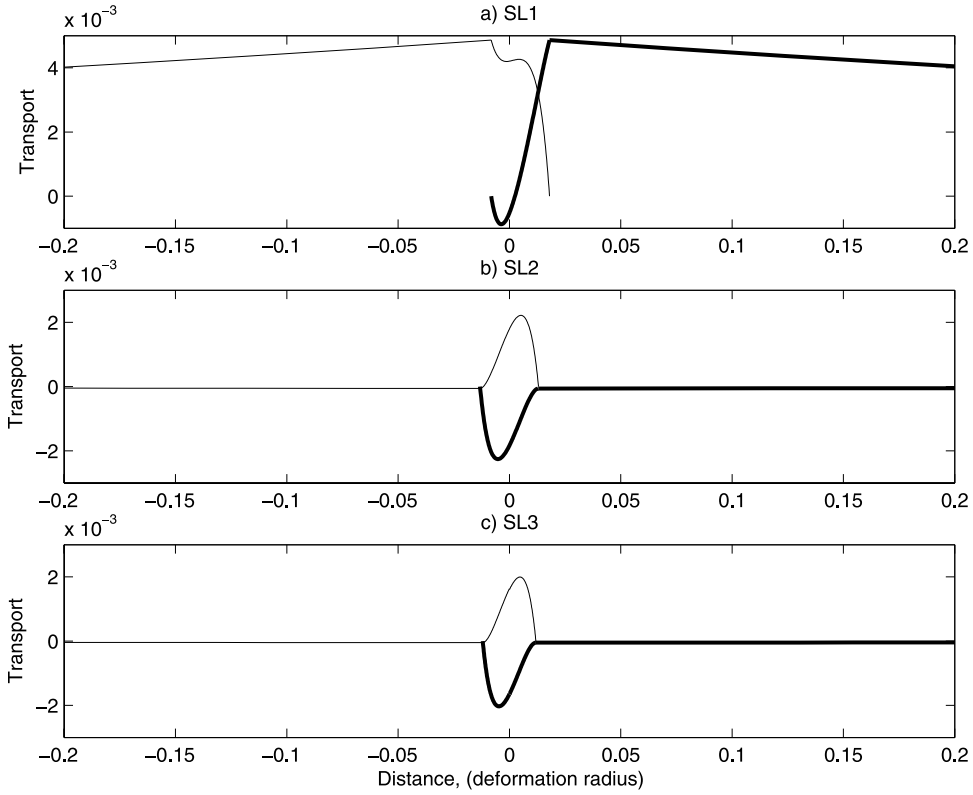

Figure 5. Nondimensional transport in water originated from the ice-free zone (thin line) and water originated from the ice-covered zone (heavy line) calculated from the layer models, for three models (a) SL1, (b) SL2, and (c) SL3 in Case A. The origin of the ordinate is the original position of the ice edge, and in its vicinity is the frontal zone of baroclinic currents with both layers in motion.

where $\dot{\eta} = d\eta/dt$ is the so-called virtual vertical velocity, which has a dimension different from the vertical velocity ordinarily used in the traditional z-coordinates. In PCOM, the bottom pressure is prognostically calculated from the bottom pressure tendency equation, which is obtained by integrating (3) from $\eta = 0$ (sea surface) to $\eta = p_B$ (bottom) and applying the corresponding boundary condition at the sea surface.

[24] For the case of evaporation/precipitation this upper boundary condition is

$$r_p \dot{\eta} = -\rho_f g Q_{E-P}. \tag{4a}$$

where ρ_f is the density of fresh water and $Q_{E\text{-}P}$ is the fresh water flux across the air-sea interface associated with evaporation and precipitation. Since p_t is the specified pressure at the upper boundary, due to the evaporation and precipitation the increment in hydrostatic pressure is $\delta(p - p_t) = -\rho_f g \delta Q_{E\text{-}P}$. The change in bottom pressure is calculated from the tendency equation, which is now in forms

$$\frac{\partial p_{bt}}{\partial t} + \nabla_2 \cdot \left(p_{bt} \vec{V}_{baro}\right) = -\rho_f g Q_{E-P} \tag{5a}$$

where $\vec{V}_{baro}$ is the vertically integrated velocity.

[25] This boundary condition is very similar to the freshwater flux boundary condition in the traditional z-coordinate model with a rigid lid, where the upper boundary is fixed at $z = 0$. However, freshwater flux due to evaporation and precipitation induces a nonzero vertical

Table 2. Volume Transport (in Sv) for the Slab Models, Case A: $H_{10} = 100\ m$, $\kappa = 0.99$, $\gamma_{SL2} = 0.99976$, $\gamma_{SL3} = 0.9998$

		Ice Zone	Frontal Zone		Ice-Free Zone	Total Flux
SL1	Upper Layer		0.065		3.2	
	Lower Layer	3.2	0.021			6.5
	Net		0.087			
SL2 ($\kappa = 1$)	Upper Layer		0.021		−0.039	
	Lower Layer	−0.039	−0.023			−0.079
	Net		−0.002			
SL3	Upper Layer		0.013	0.006	−0.032	
	Lower Layer	−0.033	−0.005	−0.013		−0.066
	Net		0.008	−0.007		

Table 3. Volume Transport (in Sv) for Case B: $H_{10} = 1000\ m$, $\kappa = 0.999$ $\gamma_{SL2} = 0.999976$ $\gamma_{SL3} = 0.99998$

		Ice Zone	Frontal Zone		Ice-Free Zone	Total Flux
SL1	Upper Layer		0.36		32.4	
	Lower Layer	32.4	−0.09			65.0
	Net		0.27			
SL2 ($\kappa = 1$)	Upper Layer		0.22		−0.39	
	Lower Layer	−0.39	−0.22			−0.79
	Net		−0.00			
SL3	Upper Layer		0.13	0.06	−0.32	
	Lower Layer	−0.34	−0.06	−0.13		−0.66
	Net		0.07	−0.07		

velocity in the rigid-lid model $w = dz/dt = E - P \neq 0$ across the upper surface [*Huang*, 1993].

[26] For the case with ice formation, the equivalent freshwater flux term is reduced to the ice formation rate; thus, the upper boundary condition for the water component of the coupled model is

$$r_p \dot{\eta} = -g \frac{\partial(\rho_i h_i)}{\partial t}, \tag{4b}$$

and the corresponding tendency equation is

$$\frac{\partial p_{bt}}{\partial t} + \nabla_2 \cdot \left(p_{bt} \vec{V}_{baro}\right) = -g \frac{\partial(\rho_i h_i)}{\partial t}. \tag{5b}$$

The pressure at the upper surface of seawater is now time-dependent

$$\frac{\partial p_t}{\partial t} = g \frac{\partial(\rho_i h_i)}{\partial t} \tag{6}$$

[27] Although the bottom pressure may indirectly change due to mass redistribution associated with baroclinic current induced by salt rejection during sea ice formation, there is no change of bottom pressure directly linked to sea ice formation.

3.2. Upper Boundary Condition for Salinity

[28] For the case with evaporation and precipitation, freshwater flux gives rise to an advective salt flux that exactly cancels the turbulent salt flux at the air-sea interface; thus, there is no net salt flux across the air-sea interface

$$0 = F^S = F^S_{Dif} - F^S_{Adv} = \frac{\rho^2 g^2}{r_p} \kappa_\nu \frac{\partial S}{\partial \eta} + g \rho_f S Q_{E-P} \tag{7a}$$

where κ_ν is the vertical diffusion coefficient for salinity, S is the salinity at the sea surface. Note that the sea surface is defined as $\eta = 0$ in the pressure-η coordinate; thus, at the air-sea interface the advective salt flux associated with evaporation (precipitation) is defined as negative (positive). This is the same as the natural boundary condition of no net salt flux across the air-sea interface, discussed by *Huang* [1993].

[29] For the case of ice formation, some of the salt in seawater is frozen into ice, i.e., the salt rejection is incomplete. Equation (6) describes the time rate of pressure at the water-ice interface. The salt flux through the water-ice interface consists of two components. The first component is included in the pressure change term (6); and there is an additional salt flux across the water-ice interface

$$F^S = F^S_{Dif} - F^S_{Adv} = \frac{\partial}{\partial t}[(S_{w1} - S_i)\rho_i h_i] \tag{7b}$$

where S_{w1} is salinity for the seawater below ice, and S_1 is the salinity of sea ice. This boundary condition reflects the physics that salt rejection during ice formation increases the salt content in the seawater below.

[30] If there is no salt rejection, $S_1 = S_{w1}$, equation (7b) leads to a statement that there is no additional salt flux across the water-ice interface; thus, salinity in seawater remains unchanged. On the other hand, if $S_1 < S_{w1}$, equation (7b) indicates an increase of salinity for the water below ice.

[31] The traditional boundary condition widely used in Boussinesq models is to treat the dynamical effect of ice formation (melting) in terms of the equivalent virtual salt flux applied to the salt balance equation

$$\kappa_S \frac{\rho_0^2 g}{r_h} \frac{\partial S}{\partial \eta} = \overline{(S_{ref} - S_i)} \frac{\partial}{\partial t}[\rho_i h_i] \tag{8}$$

where $\overline{S_{ref} - S_i}$ is the difference between the mean reference salinity and salinity of sea ice. Boundary condition (8) is equivalent to the virtual salt flux condition used in the traditional z-coordinates model [e.g., *Roullet and Madec*, 2000; *Tartinville et al.*, 2001; *Prange and Gerdes*, 2006]. Note that during the ice formation there is no change in the total volume of seawater in the model ocean. As discussed by *Huang* [1993], relatively low salinity is related to precipitation, or ice melting in the ice-covered ocean; thus, a virtual salt flux condition based on the local salinity of seawater can lead to a net gain of salinity in the model ocean. As a compromise, virtual salt flux condition used in a model must be based on the mean reference salinity. For the simulation of the world ocean circulation, the reference salinity should be set to 35; however, the surface salinity in the Arctic can be as low as 30. Assuming sea ice salinity is 5, thus, $\overline{S_{ref} - S_i} = 30$. On the other hand, the corresponding factor in equation (7b) is based on the local salinity of seawater and sea ice, $S_{w1} - S_i = 25$. At some locations the difference between the in situ seawater salinity and the young sea ice can be even smaller. Therefore, similar to the case of evaporation and precipitation, the virtual salt flux condition tends to exaggerate the dynamic effect of freshwater flux forcing, so the natural boundary condition is a more accurate way to simulate the problem associated with ice formation.

[32] In addition, as discussed by *Huang and Jin* [2002], the net change in bottom pressure produced by virtual salt flux is misinterpreted; however, this is beyond of the scope of this study.

4. Results From Numerical Experiments

[33] We have carried out numerical experiments based on PCOM (for Cases C, D, and E) and BCOM (for Case F), coupled to a sea ice model. The sea ice model is a simple thermodynamics model formulated according to Parkinson and Washington (1979). The ocean and ice are coupled through heat flux and freshwater flux due to ice freezing (melting) and through hydrostatic pressure through the water column; however, there is no other dynamic interactions between water and ice.

[34] The restoring boundary condition is applied to the temperature. The surface heat flux is

$$F_h = D(T^* - T) * (1 - A) \tag{9}$$

where $D = 40W/m^2/K$, $T^* = -20°C$ for the northern half of the model basin, and it is $T^* = -1.638°C$ for the southern half of the model ocean, A is the ice concentration.

[35] In the following numerical experiments, the model ocean is 1000 m deep on an f-plane, with $f = 1.5 \times 10^{-4}/s$ (corresponding to a high latitude ocean), with 30 layers of uneven thickness, with fine resolution in the upper ocean. The seawater has a uniform temperature of $-1.638°C$ and salinity of 30. There is no wind stress or freshwater flux at the upper surface. At the initial time the model ocean is at rest. Sea ice is formed when the northern half of the model ocean is subjected to a sudden cooling (here $T^* = -20°C$), started at time t = 0. For all four cases, 1 m of seawater is frozen into ice. It took about two weeks for the ice thickness to reach 1 m (of the equivalent water thickness). Salinity of ice is set to 5, except for Case C where $S_i = 30$, the same as the seawater.

4.1. Case C

[36] (1) Ice formation is treated as a virtual vertical velocity in equation (4b). (2) Pressure at the water-ice interface increases as equation (6), indicating the certain amount of water is transformed into sea ice. At the same time, there is no net salt flux leaving the ocean, controlled by equation (7b). As a result, there is no salinity change for the water column below the sea ice.

[37] The numerical model produced an ocean circulation with a net volume transport of less than 0.003 Sv, and this nonzero flow solution is apparently due to some truncation errors in the numerical model, and can be omitted.

4.2. Case D

[38] Same as Case C, except $S_i = 30$. There is a salt rejection and salinity for the water column below the sea ice increases accordingly. The numerical model produced an ocean circulation with a net volume transport of -0.63 Sv, which is very close to the value (-0.66 Sv) predicted by SL3 in section 2. This slightly smaller value in the numerical experiment is due to the fact that our numerical experiments were confined to a finite domain.

4.3. Case E

[39] (1) Ice formation is treated as a virtual vertical velocity in equation (4b). (2) Pressure at the water-ice interface remains unchanged, i.e., we ignored pressure increase described in equation (6).

[40] There is a salt rejection and the net salt flux into the water column below ice is controlled by equation (7b). The numerical model produced an ocean circulation with a net volume transport of 64.77 Sv, which is slightly smaller than the value (-65 Sv) predicted by SL1 in section 2. This slightly smaller value is due to the finite domain used in the model.

4.4. Case F

[41] Ice formation is treated in terms of the virtual salt flux condition (8). The numerical experiment produced an ocean circulation with a net volume transport of less than -0.74 Sv, which is slightly smaller than the value (-0.79 Sv) predicted by SL2 in section 2. This slightly reduction of volume flux is again due to the finite domain used in the model.

[42] Note that although the time-dependent part of the adjustment process is omitted in the analytical models, it is included in the numerical experiments based on OGCM, and final results from these two approaches are virtually the same. Therefore, the friction effect neglected in the analytical model for the adjustment problem is not critically important in terms of the final state of circulation induced by ice formation.

[43] For example, the meridional views of the solution after the adjustment induced by 1-m ice formation distribution for Case D, Figures 6 and 7, are similar to that obtained from the slab model SL3, Figures 4 and 5. Since the model has a continuous stratification, the ice-edge velocity front in the numerical model includes a vertical structure (Figure 7) which is not resolved in the slab model. Structure of the free surface elevation and current obtained for Case F are similar to that produced from the slab model SL1, Figure 8.

5. Conclusion

[44] This study is focused on the suitable kinematical boundary conditions dealing the freshwater and salt fluxes through the ice-water interface. We have provided simple analytical solutions which may be used to test whether an ocean-ice coupled model simulate the property exchanges through the water-ice interface accurately. The answer is simple: if the model runs without salt rejection, then sea ice formation in an originally stagnant ocean should not produce any detectable currents. With the salt rejection included in the model run, ice formation can induce a weak baroclinic flow near the ice edge and an extremely weak barotropic flow in the far field.

[45] A potential application of the boundary conditions discussed in this note is to examine why some of the oceanic circulation models in the AOMIP (Arctic Ocean Model Intercomparison Project [*Proshutinsky et al.*, 2001]) develop flow patterns that go in direction exactly opposite to the direction inferred from observations. *Yang* [2006] has provided an argument based on the balance of potential vorticity in the basin. In some sense, the exchanges of water and salt through the water-ice edge are important items in

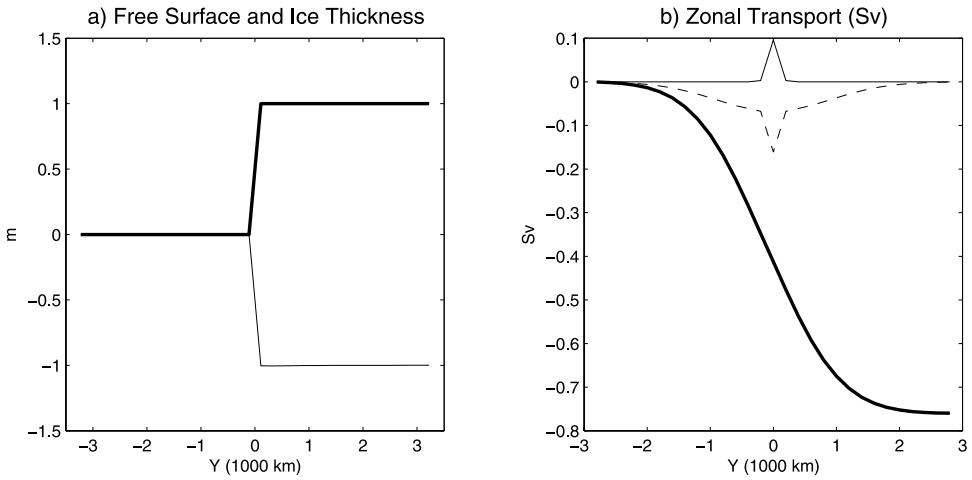

Figure 6. Final circulation after ice formation obtained from Case B. (a) Ice thickness (heavy line) and free surface of seawater (thin line). (b) Zonal transport, thin (dashed) line for the vertically integrated eastward (westward) transport per each grid (200 km wide), and the heavy line for the total accumulated zonal transport, integrated from the southern boundary.

the potential vorticity budget. It seems very interesting to check whether different formulations of boundary condition at the water-ice interface can affect the pattern of the basin-scale circulation in the Arctic Ocean.

[46] Note that the incorrect way of handling the upper boundary conditions associated with sea ice formation/melting may also affect the capability of the model in predicting the bottom pressure and the angular inertia of the Earth [*Huang and Jin*, 2002].

[47] Our discussion here is focused on the case with the pressure-η coordinate model; however, the suitable boundary conditions for other coordinates can be derived accordingly. For example, in the traditional z-coordinate model, the natural boundary condition for ice formation should be parameterized as an increase of hydrostatic pressure on the upper surface of the water column and a reduction of the upper most grid thickness. This can be easily carried out for models in z-σ coordinate. On the other hand, in the traditional z-coordinate model, the sea ice may be treated as 'top topography' in the upper surface of the model ocean. Such 'top topography' changes its shape (the thickness of sea ice) with time, and this should be simulated accurately.

[48] Our discussion in this paper is confined to the case of a model ocean with no mean current and it is coupled to a

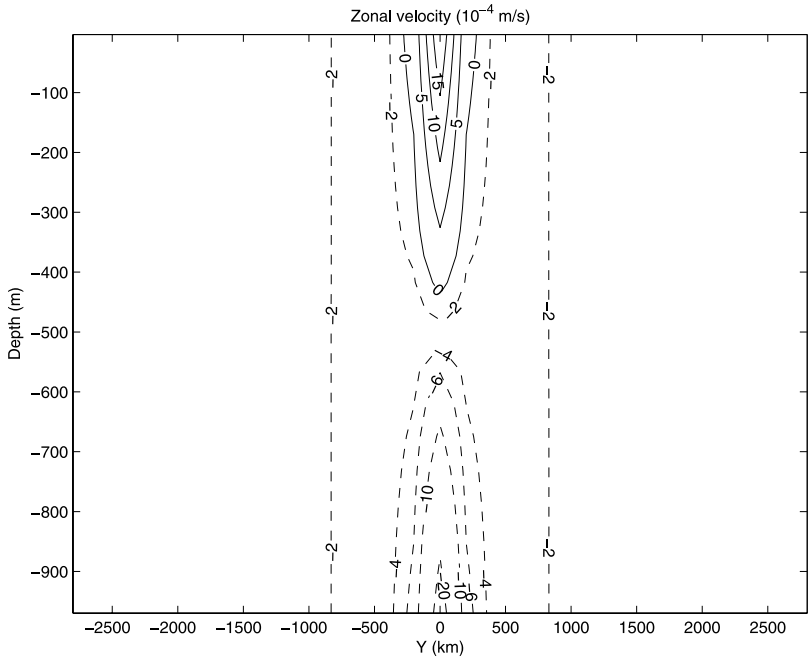

Figure 7. Vertical distribution of zonal velocity obtained from Case B, in units of 10^{-4} *m/s*.

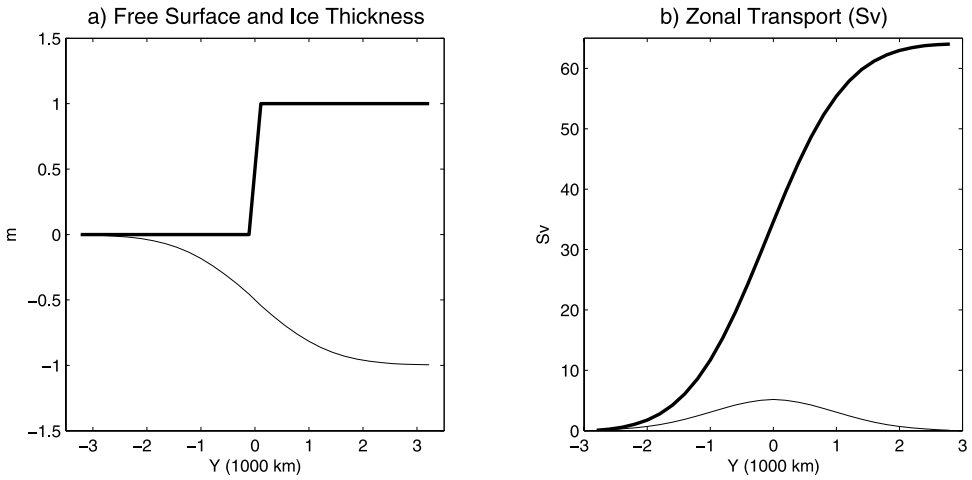

Figure 8. Final circulation after ice formation obtained from Case C. (a) Ice thickness (heavy line) and free surface of seawater (thin line). (b) Zonal transport, thin line for the vertically integrated eastward transport per each grid (200 km wide), and the heavy line for the total accumulated zonal transport, integrated from the southern boundary.

thermodynamic ice model only. In reality, there is a net production of sea ice in the Arctic Ocean, the horizontal transport of sea ice may enhance the production of sea ice and intensify the freshwater/flux fluxes into the ocean [e.g., *Zhang et al.*, 2003]. As a result, the potential errors introduced by the inaccurate boundary conditions for freshwater/salt fluxes through the water-ice interface may be further amplified. Therefore, more careful handling of such boundary conditions may help us to improve the model's capability of simulation the oceanic circulation in the world oceans, especially in the Arctic Ocean.

Appendix A: Ice Formation in the Slab Models

A1. A Model Without Salt Rejection (SL0)

[49] We will treat the space which is actually occupied by sea ice as an empty space which will be filled with seawater flowing horizontally. Assumed that a slab of seawater, h_w, is suddenly transformed to sea ice, a step-like feature is thus created at the initial time, Figure 1a. The final results of the adjustment for this case is classic; however, we include the solution here for the completeness of this study.

[50] Assume the flow is independent of x, the x-momentum equation is $du/dt = fv$, where u and v are horizontal velocity, and f is the Coriolis parameter. Integration from $t = 0$ to ∞ leads to

$$u = f(y - Y) + U(Y), \tag{A1}$$

where Y and U are the initial position and velocity of water parcels, and U will be assumed to be zero for this study. In the final state, the downstream velocity is geostrophic:

$$fu = -gh_y. \tag{A2}$$

Conservation of mass in this layer gives

$$h = HdY \;/\; dy, \tag{A3}$$

where H is the initial layer thickness. Note that there are two regions, I and II, after adjustment because of the different initial layer thickness, Figure 1b.

[51] Combining equations (A1), (A2), and (A3) leads to

$$\frac{gH}{f^2}\frac{d^2Y}{dy^2} - Y = -y \tag{A4}$$

[52] Region I: the initial layer thickness is H_{10}. We will introduce the nondimensional variable

$$(y, Y) = (y', Y') \cdot \lambda,$$

where $\lambda = \sqrt{gH_{10}}\,/f$ is the deformation radius. Dropping the prime, the governing equation (A4) is reduced to

$$\ddot{Y} - Y = -y \tag{A5}$$

where the dots indicate the second derivative with respect to y. The solution which is bounded at $-\infty$ is

$$Y_I = y + c_1 \cdot e^y \tag{A6}$$

[53] Region II: the initial layer thickness is κH_{10}, the equation corresponding to (A5) is

$$\kappa\ddot{Y} - Y = -y \tag{A7}$$

and the solution which is bounded at ∞ is

$$Y_{II} = y + c_2 e^{-y/\sqrt{\kappa}} \tag{A8}$$

[54] Since the choice of the origin of the y-coordinate is arbitrary, we choose $y = 0$ as the position of the interface between regions I and II. Therefore, the matching conditions at $y = 0$ are (1) continuity of the water parcel position Y: $c_1 = c_2$, and (2) continuity of layer thickness h: $1 + c_1 = \kappa(1 - c_2/\sqrt{\kappa})$.

[55] From these two relations, we obtain the solution: $c_1 = c_2 = c = (\kappa - 1)/(1 + \sqrt{\kappa})$. Note that $\kappa = 1 - h_w/H_{10} = 1 - r$, where $r \bullet 1$; thus, $c \bullet -r/2$, $|c| \bullet 1$.

[56] Due to the Coriolis force, water parcels gain westward momentum during their southward movement, and the total transport in region I can be found by integration:

$$\int_{-\infty}^{0} h_1 u_1 dy = -f\lambda^2 c H_{10}(1 + c/2) \tag{A9a}$$

Similarly, total transport in region II is

$$\int_{0}^{\infty} h_2 u_2 dy = -f\lambda^2 c H_{10}\kappa\left(\sqrt{\kappa} - \frac{c}{2}\right) \tag{A9b}$$

The total transport within the resulted frontal current is

$$M = -f\lambda^2 c H_{10}\left[1 + \frac{c}{2} + \kappa\left(\sqrt{\kappa} - \frac{c}{2}\right)\right] \bullet g H_{10} h_w / f \tag{A10}$$

Note that the horizontal scale of this geostrophic adjustment is on the order of the barotropic radius of deformation. Since ice formation happens at high latitudes, we take the nominal value as $f = 1.5 \cdot 10^{-4}\ s^{-1}$. Assuming an ocean is 1000 m deep, and 1 m of water is frozen to be ice, the corresponding volume flux associated with the front is approximately 65 Sv.

[57] However, this analysis omits the contribution due to salt rejection. As will be shown shortly, salt rejection induces a pressure force against the movement of seawater towards the ice-formation region; thus, the volume flux associated with the adjustment is charged, according to the model adapted for the dynamical processes involved.

A2. Slab Model 1 (SL1)

[58] In the traditional practice of ice formation based on the z-coordinate, the space occupied by seawater in the model ocean remains the same, regardless of whether ice is formed or not. In a sense, the same space has been counted twice: first as ice, and second as water. In some recent model study, the natural boundary condition [*Huang*, 1993], which was proposed for evaporation and precipitation, was interpreted as a boundary condition for sea ice formation as follows. When a layer of seawater δh is frozen during a time interval of δt, an "equivalent" upward velocity $\delta h/\delta t$ is specified as an upper boundary condition for the model ocean, and at the same time the upper surface of water still occupies the same space. This case will be referred as SL1.

[59] Assume ice is instantaneously formed, then this boundary condition for sea ice formation can be idealized as a remove of a slab of water at time $t = 0$, as shown in Figure 2a. Because of salt rejection during ice formation, salinity and total mass of the water below sea ice is increased compared with the case where there is no salt rejection, and the water column height is slightly enlarged to κH_{10}. This increase is very small and negligible, as shown in Appendix B, thus we have.

$$\kappa = 1 - (h_w + \delta h)/H_{10} = 1 - r,$$
$$r = (h_w + \delta h)/H_{10} \bullet h_w/H_{10} \bullet 1.$$

During the adjustment, water from ice-free regime spreads over water from ice-covered regime with slightly higher density. There are three regions in the final state, Figure 2b, which structure is discussed as follows.

[60] (1) Region I: There is the upper layer only. The basic equation is the same as equation (A4). Introducing the same nondimensional variable $(y, Y) = (y', Y') \cdot \lambda$, this equation is reduced to equation (A5), and the solution which is finite at infinity is

$$Y_{1,I} = y + A \cdot e^{y}, h_{1,I} = H_{10}(1 + Ae^{y}) \tag{A11}$$

[61] (2) Region II: There are two moving layers. Assume the flow is independent of x, the x-momentum equations for a the upper and lower layers are

$$\frac{du_1}{dt} = f\nu_1,\ \frac{du_2}{dt} = f\nu_2 \tag{A12}$$

where u_1, u_2, v_1, and v_2 are horizontal velocity in the upper and lower layers, and f is the Coriolis parameter. Upon integration from $t = 0$ to ∞, these lead to

$$u_1 = f(y - Y_1), u_2 = f(y - Y_2) \tag{A13}$$

where Y_1 and Y_2 are the initial positions of the water parcels.

[62] In the final state, the downstream velocities are geostrophic:

$$fu_1 = -g\left(h_{1y} + h_{2y}\right),\ fu_2 = -g\left(\gamma h_{1y} + h_{2y}\right) \tag{A14}$$

where $\gamma = \rho/(\rho + \Delta\rho) < 1$. Density change due to salt rejection is discussed in Appendix B. Conservation of mass in each layer gives

$$h_1 = H_1 \frac{dY_1}{dy},\ h_2 = H_2 \frac{dY_2}{dy} \tag{A15}$$

where $H_1 = H_{10}$ and $H_2 = \kappa H_{10}$ are the initial thickness of these two layers.

$$\frac{gH_{10}}{f^2}\left(\frac{d^2Y_1}{dy^2} + \kappa\frac{d^2Y_2}{dy^2}\right) - Y_1 = -y \tag{A16a}$$

$$\frac{gH_{10}}{f^2}\left(\gamma\frac{d^2Y_1}{dy^2} + \kappa\frac{d^2Y_2}{dy^2}\right) - Y_2 = -y \tag{A16b}$$

Introducing the new variables

$$(y, Y_1, Y_2) = \left(y', Y_1', Y_2'\right) \cdot \lambda, \tag{A17}$$

equations (A16a) and (A16b) are reduced to

$$\ddot{Y}_1 + \kappa\ddot{Y}_2 - Y_1 = -y \tag{A18a}$$

$$\gamma\ddot{Y}_1 + \kappa\ddot{Y}_2 - Y_2 = -y \tag{A18b}$$

The corresponding solutions in this region are

$$Y_{1,II} = y + a_1 \sinh(\alpha_+ y) + a_2 \cosh(\alpha_+ y) + a_3 \sinh(\alpha_- y) + a_4 \cosh(\alpha_- y) \quad \text{(A19a)}$$

$$Y_{2,II} = y + b_1 \sinh(\alpha_+ y) + b_2 \cosh(\alpha_+ y) + b_3 \sinh(\alpha_- y) + b_4 \cosh(\alpha_- y) \quad \text{(A19b)}$$

$$h_{1,II} = H_{10}[1 + a_1\alpha_+ \cosh(\alpha_+ y) + a_2\alpha_+ \sinh(\alpha_+ y) + a_3\alpha_- \cosh(\alpha_- y) + a_4\alpha_- \sinh(\alpha_- y)] \quad \text{(A19c)}$$

$$h_{2,II} = \kappa H_{10}[1 + b_1\alpha_+ \cosh(\alpha_+ y) + b_2\alpha_+ \sinh(\alpha_+ y) + b_3\alpha_- \cosh(\alpha_- y) + b_4\alpha_- \sinh(\alpha_- y)] \quad \text{(A19d)}$$

where the exponential indices satisfy

$$\alpha_\pm = \left[\frac{(\kappa+1) \pm \sqrt{(\kappa-1)^2 + 4\kappa\gamma}}{2\kappa(1-\gamma)}\right]^{1/2} \quad \text{(A20)}$$

[63] (3) Region III: There is the lower layer only. The solution which is finite at ∞ is the same as discussed in equation (A8), i.e.,

$$Y_{2,III} = y + B \cdot e^{-y/\sqrt{\kappa}}, h_{2,III} = \kappa H_{10}\left(1 - \frac{B}{\sqrt{\kappa}} e^{-y/\sqrt{\kappa}}\right) \quad \text{(A21)}$$

Since the choice of the coordinates is arbitrary, we set y = 0 as the boundary between regions III and II, and the boundary between regions II and I is denoted as y_-. In order to find the final solutions, we have to determine 11 unknown, a_1, a_2, a_3, a_4, b_1, b_2, b_3, b_4, A, B, and y_-.

[64] First, solutions (A19a)–(A19d) should satisfy equations (A18a) and (A18b); thus, we have the following relations

$$b_1 = \frac{\gamma\alpha_+^2}{1-k\alpha_+^2} a_1, b_2 = \frac{\gamma\alpha_+^2}{1-k\alpha_+^2} a_2, b_3 = \frac{\gamma\alpha_-^2}{1-k\alpha_-^2} a_3, \quad b_4 = \frac{\gamma\alpha_-^2}{1-k\alpha_-^2} a_4 \quad \text{(A22)}$$

Second, at $y = y_-$, Y_1 and h_1 are continuous, and $h_2 = 0$:

$$a_1 \sinh(\alpha_+ y_-) + a_2 \cosh(\alpha_+ y_-) + a_3 \sinh(\alpha_- y_-) + a_4 \cosh(\alpha_- y_-) = Ae^{y_-} \quad \text{(A23)}$$

$$a_1\alpha_+ \cosh(\alpha_+ y_-) + a_2\alpha_+ \sinh(\alpha_+ y_-) + a_3\alpha_- \cosh(\alpha_- y_-) + a_4\alpha_- \sinh(\alpha_- y_-) = Ae^{y_-} \quad \text{(A24)}$$

$$b_1\alpha_+ \cosh(\alpha_+ y_-) + b_2\alpha_+ \sinh(\alpha_+ y_+) + b_3\alpha_- \cosh(\alpha_- y_-) + b_4\alpha_- \sinh(\alpha_- y_-) = -1 \quad \text{(A25)}$$

Third, at $y = 0$, Y_2 and h_2 are continuous, and $h_1 = 0$:

$$b_2 + b_4 = B \quad \text{(A26)}$$

$$b_1\alpha_+ + b_3\alpha_- = -B/\sqrt{\kappa} \quad \text{(A27)}$$

$$a_1\alpha_+ + a_3\alpha_- = -1 \quad \text{(A28)}$$

Finally, the last constraint is that the original position of the right edge of the upper layer should be the same as the left edge of the lower layer, i.e., $Y_{1,II}(0) = Y_{2,II}(y_-)$, or

$$y_- + b_1 \sinh(\alpha_+ y_-) + b_2 \cosh(\alpha_+ y_-) + b_3 \sinh(\alpha_- y_-) + b_4 \cosh(\alpha_- y_-) = a_2 + a_4 \quad \text{(A29)}$$

These relations can be used to determine all the unknown coefficients and the position of the boundary y_0.

[65] Note that the original position of ice edge should be equal to $Y_{1,II}(0)$, and this will be used to shift the origin of the ordinate in plotting the final solution. The corresponding volume flux per unit length in the x-direction is

$$V = hu = fH_{10}\lambda v, \quad \text{(A30)}$$

where $v = (y - Y)\dfrac{dY'}{dy'}$ is the nondimensional volume flux.

A3. Slab Model 2 (SL2)

[66] Note that a small modification of the SL1 can be used for the case when the ice formation is simulated in terms of the so-called virtual salt flux. Instead of specifying a freshwater flux leaving the model ocean, one can use a model formed in the traditional Boussinesq approximation. In such a model, the total volume of seawater remains unchanged during the ice formation, and the only effect of ice formation on the model is the salt rejection. The same formulation discussed in this section can be used for such a model, with the same γ; however, the layer thickness ratio is now set to $\kappa = 1$. Such a model will be referred as the SL2.

A4. Slab Model 3 (SL3)

[67] When sea ice is formed without salt rejection, there is no horizontal pressure gradient at the level below the ice, so ice formation without salt rejection does not induce horizontal motion in the ocean.

[68] After salt rejection from the newly formed ice, water below the ice is slightly saltier than its environments, and this unbalance initial baroclinic pressure can induce a baroclinic circulation in the ocean, Figure 3. Due to the outward motions of the slightly saltier water in the ice formation regime, the free surface of the ice-free regime is very slightly pushed upward near the ice edge, Figure 3b. However, as will be shown this baroclinic circulation is relatively weak. This case will be referred as model SL3.

[69] The final solutions consist of four regions, Figure 3b. The dynamics in regions I and II are the same as discussed in the second case in the previous section. There is a new region III, where water flows under sea ice and it is near the ice edge, Figure 3b. In this region, the basic equations and

the general solutions of the equations are the same as in region II.

$$Y_{1,III} = y + c_1 \sinh(\alpha_+ y) + c_2 \cosh(\alpha_+ y) + c_3 \sinh(\alpha_- y) + c_4 \cosh(\alpha_- y) \quad \text{(A31a)}$$

$$Y_{2,III} = y + d_1 \sinh(\alpha_+ y) + d_2 \cosh(\alpha_+ y) + d_3 \sinh(\alpha_- y) + d_4 \cosh(\alpha_- y) \quad \text{(A31b)}$$

In region IV, there is only the lower layer, so solution is the same as discussed in previous section,

$$Y_{2,IV} = y + B \cdot e^{-y/\sqrt{\kappa}} \quad \text{(A32)}$$

[70] In the present case, we will choose the edge of sea ice as the origin of the coordinates, $y = 0$, and the boundary between regions I and II as y_-, boundary between regions III and IV as y_+. This problem has 20 unknown, a_i, b_i, c_i, d_i, $i = 1, 2, 3, 4$; A, B, y_-, y_+; thus, 20 constraints are required.

[71] First, solution $Y_1$and Y_2 should satisfy the basic equations (A18a) and (A18b); thus, there are four relations:

$$b_1 = \frac{\gamma\alpha_+^2}{1 - k\alpha_+^2} a_1,\ b_2 = \frac{\gamma\alpha_+^2}{1 - k\alpha_+^2} a_2,\ b_3 = \frac{\gamma\alpha_-^2}{1 - k\alpha_-^2} a_3,$$
$$b_4 = \frac{\gamma\alpha_-^2}{1 - k\alpha_-^2} a_4 \quad \text{(A33)}$$

$$d_1 = \frac{\gamma\alpha_+^2}{1 - k\alpha_+^2} c_1,\ d_2 = \frac{\gamma\alpha_+^2}{1 - k\alpha_+^2} c_2,\ d_3 = \frac{\gamma\alpha_-^2}{1 - k\alpha_-^2} c_3,$$
$$d_4 = \frac{\gamma\alpha_-^2}{1 - k\alpha_-^2} c_4 \quad \text{(A34)}$$

[72] Second, at $y = y_-$, Y_1 and h_1 are continuous, and $h_2 = 0$:

$$a_1 \sinh(\alpha_+ y_-) + a_2 \cosh(\alpha_+ y_-) + a_3 \sinh(\alpha_- y_-) + a_4 \cosh(\alpha_- y_-) = A e^{y_-} \quad \text{(A35)}$$

$$a_1\alpha_+ \cosh(\alpha_+ y_-) + a_2\alpha_+ \sinh(\alpha_+ y_-) + a_3\alpha_- \cosh(\alpha_- y_-) + a_4\alpha_- \sinh(\alpha_- y_-) = A e^{y_-} \quad \text{(A36)}$$

$$b_1\alpha_+ \cosh(\alpha_+ y_-) + b_2\alpha_+ \sinh(\alpha_+ y_-) + b_3\alpha_- \cosh(\alpha_- y_-) + b_4\alpha_- \sinh(\alpha_- y_-) = -1 \quad \text{(A37)}$$

[73] Third, at $y = y_+$, Y_2 and h_2 are continuous, and $h_1 = 0$

$$d_1 \sinh(\alpha_+ y_+) + d_2 \cosh(\alpha_+ y_+) + d_3 \sinh(\alpha_- y_+) + d_4 \cosh(\alpha_- y_+) = B e^{-y_+/\sqrt{\kappa}} \quad \text{(A38)}$$

$$d_1\alpha_+ \cosh(\alpha_+ y_+) + d_2\alpha_+ \sinh(\alpha_+ y_+) + d_3\alpha_- \cosh(\alpha_- y_+) + d_4\alpha_- \sinh(\alpha_- y_+) = -B(\kappa)^{-1/2} e^{-y_+/\sqrt{\kappa}} \quad \text{(A39)}$$

$$c_1\alpha_+ \cosh(\alpha_+ y_+) + c_2\alpha_+ \sinh(\alpha_+ y_+) + c_3\alpha_- \cosh(\alpha_- y_+) + c_4\alpha_- \sinh(\alpha_- y_+) = -1 \quad \text{(A40)}$$

Forth, at y = 0, Y_1, Y_2, h_2 are continuous

$$a_2 + a_4 = c_2 + c_4 \quad \text{(A41)}$$

$$b_2 + b_4 = d_2 + d_4 \quad \text{(A42)}$$

$$b_1\alpha_+ + b_3\alpha_- = d_1\alpha_+ + d_3\alpha_- \quad \text{(A43)}$$

In addition, pressure in the upper layer should be continuous at y = 0, $h_{1,II}(0) - h_{1,III}(0) = h_i\rho_i / \rho$, or

$$a_1\alpha_+ + a_3\alpha_- - (c_1\alpha_+ + c_3\alpha_-) = \rho_i h_i / \rho H_{10}; \quad \text{(A44)}$$

Finally, the position in the original coordinate of the left edge of the upper layer and the right edge of the lower layer should be the same as the ice edge:

$$y_+ + c_1 \sin h(\alpha_+ y_+) + c_2 \cosh(\alpha_+ y_+) + c_3 \sinh(\alpha_- y_+) + c_4 \cosh(\alpha_- y_+) = 0 \quad \text{(A45)}$$

$$y_- + b_1 \sin h(\alpha_+ y_-) + b_2 \cosh(\alpha_+ y_-) + b_3 \sinh(\alpha_+ y_-) + b_4 \cosh(\alpha_- y_-) = 0 \quad \text{(A46)}$$

[74] Equations (A41) and (A42) lead to simple relations: $c_2 = a_2$ and $c_4 = a_4$. Thus, equations (A33)–(A44) can be reduced to a set of six equations which is linear in variables a_1; a_2; a_3; a_4; c_1; c_3; but nonlinear in y_- and y_+. Combining these six equations with equations (A45) and (A46), all these unknowns can be determined.

Appendix B: Changes in Water Properties Due to Sea Ice Formation

[75] Assume seawater properties are: density ρ, salinity S; salinity of sea ice is S_i, the depth of ocean is H, where a slab of water, h_w, is frozen; thus, the depth of water below sea ice is $H_2 = h - h_w$. Total amount of salt ejected from ice: $h_w\rho\,(S - S_i)/1000$. After salt rejection the new salinity in water below ice is:

$$S + \Delta S = \frac{H_2\rho S + h_w\rho(S - S_i)}{H_2\rho + h_w\rho(S - S_i)/1000} \bullet S\left[1 + \frac{h_w}{H_2}\left(1 - \frac{S_i}{S}\right)\right] \cdot \left(1 - \frac{h_w}{H_2}\frac{S - S_i}{1000}\right)$$

$$\Delta S \bullet S\frac{h_w}{H_2}\left(1 - \frac{S_i}{S} - \frac{S - S_i}{1000}\right).$$

Assume $h_w = 1\ m$, $H_2 = 1000\ m$, $S = 30$, $S_i = 4$, we have $\Delta S \bullet 0.025$.

[76] Density difference is $\Delta\rho/\rho = \beta\Delta S \bullet 8{\cdot}10^{-4} \cdot 0.025 = 2{\cdot}10^{-5}$. Changes in layer thickness: $\Delta h = \dfrac{\Delta M - H_2\Delta\rho}{\rho} =$

$\frac{h_w(S-S_i)}{1000} - H_2\frac{\Delta\rho}{\rho}$. For the case discussed above, we have the estimate: $\Delta h \bullet 0.03 - 0.024 = 0.006\ m$. Thus, the second layer will become slightly thicker, but this change is very small, and may be negligible. For the case of a virtual salt flux condition, the global mean salinity 35 should be used, and the corresponding values are: $\Delta S = 25$, $\Delta\rho/\rho \bullet 2.4{\cdot}10^{-5}$.

[77] **Acknowledgments.** This study was supported by the Institute of Ocean and Climate Change Institute of Woods Hole Oceanographic Institution. Jiayan Yang and Andrey Proshutinsky provided intellectual stimulation during this study. Xiangdong Zhang, an anonymous reviewer, and editor's comments helped to improve the presentation of this paper.

References

Goldsbrough, G. (1933), Ocean currents produced by evaporation and precipitation, *Proc. R. Soc. London, Ser. A*, *141*, 512–517.

Huang, R. X. (1993), Real freshwater flux as a natural boundary condition for the salinity balance and thermohaline circulation forced by evaporation and precipitation, *J. Phys. Oceanogr.*, *23*, 2428–2446.

Huang, R. X., and X.-Z. Jin (2002), Sea surface elevation and bottom pressure anomalies due to thermohaline forcing: Part I: isolated perturbations, *J. Phys. Oceanogr.*, *32*, 2131–2150.

Huang, R. X., and X.-Z. Jin (2007), Gravitational potential energy balance for the thermal circulation in a model ocean, *J. Phys. Oceanogr.*, *36*, in press.

Huang, R. X., and R. W. Schmitt (1993), The Goldsbrough-Stommel circulation of the world oceans, *J. Phys. Oceanogr.*, *23*, 1277–1284.

Huang, R. X., X.-Z. Jin, and X.-H. Zhang (2001), An oceanic general circulation model in pressure coordinates, *Adv. Atmos. Sci.*, *18*, 1–22.

Mesinger, F., and Z. I. Janjic (1985), Problems and numerical methods of the incorporation of mountains in the atmospheric models, *Lectures Appl. Math.*, *22*, 81–120.

Mihaljan, J. M. (1963), An exact solution of the Rossby adjustment problem, *Tellus*, *15*, 150–154.

Prange, M., and R. Gerdes (2006), The role of surface freshwater flux boundary conditions in Arctic Ocean Modelling, *Ocean Modell.*, *13*, 25–43.

Proshutinsky, A. Y., et al. (2001), Multinational effort studies difference among Arctic Ocean Models, *Eos Trans. AGU*, *82*, 637–644.

Roullet, G., and G. Madec (2000), Salt conservation, free surface, and varying levels: A new formulation for ocean general circulation models, *J. Geophys. Res.*, *105*, 23,927–23,942.

Stommel, H. M. (1994), The delicate interplay between wind-stress and buoyancy input in ocean circulation: The Goldsbrough variation, *Tellus*, *36*, 111–119.

Tartinville, B., J.-M. Campin, T. Fichefet, and H. Goosse (2001), Realistic representation of the surface freshwater flux in an ice-ocean general circulation model, *Ocean Modell.*, *3*, 95–108.

Yang, J.-Y. (2006), The Artic and subartic-ocean flux of potential vorticity and Arctic Ocean circulation, *J. Phys. Oceanogr.*, *35*, 2387–2407.

Zhang, X., and J. Zhang (2001), Heat and freshwater budgets and pathways in the Arctic Mediterranean in a coupled ocean/sea-ice model, *J. Oceanogr.*, *57*, 207–234.

Zhang, X., J. E. Walsh, and M. Ikeda (2003), Arctic sea ice and freshwater changes driven by the atmospheric leading mode in a coupled sea ice-ocean model, *J. Clim.*, *16*, 2159–2177.

R. X. Huang and X.-Z. Jin, Department of Physical Oceanography, Woods Hole Oceanographic Institution, Woods Hole, MA 02543, USA. (rhuang@whoi.edu)